Eur. J. Biochem. *188*, 455–461 (1990)

NMR and molecular dynamics studies of the *mKr2* 'zinc finger'

Mark D. CARR [1], Annalisa PASTORE [2], Heinrich GAUSEPOHL [2], Rainer FRANK [2] and Paul ROESCH [1]

[1] Max-Planck-Institut für Medizinische Forschung, Abteilung Biophysik, Heidelberg, Federal Republic of Germany
[2] European Molecular Biology Laboratory, Heidelberg, Federal Republic of Germany

(Received July 26/October 23, 1989) – EJB 89 0934

We determined the structure of a 30-amino-acid 'zinc finger' motif from the mouse Kruppel-like gene *mKr2* in solution in the absence of metal ions by two-dimensional NMR, distance geometry and restrained molecular dynamics methods. The most prominent secondary structural feature of the peptide is a helix extending from Ser14 to Ile20. The zinc-containing structure of the peptide was simulated by molecular dynamics calculations with restraints derived from the known geometry of the zinc ion and the ligating amino acid residues Cys6, Cys9, His22, His26. The latter structure does not deviate markedly from the set of structures determined for the zinc-free peptide, i.e. this peptide can accommodate a Zn^{2+} ion without major structural rearrangements. Thus, we propose that the metal ion stabilizes the existing three-dimensional peptide structural motif rather than introducing novel structural features.

An increasing number of proteins believed to be involved in regulating gene expression have been shown to contain copies of a polypeptide unit approximately 30 residues long. It has the consensus sequence $(F,Y)XCX_{2or4}CX_3FX_5$-$LX_2HX_3HX_5$ and is thought to form a nucleic-acid-binding domain [1]. Portions of proteins conforming to this consensus sequence are commonly referred to as 'zinc fingers', since the nine repeats of the motif identified in *Xenopus* transcription factor IIIA have each been demonstrated to bind a single Zn^{2+}, with the conserved cysteines and histidines tetrahedrally coordinating the metal ion [2, 3]. It has also been proposed that three highly conserved phenylalanyl, leucyl and tyrosyl residues form the core of the zinc-finger structure [2].

Two models of the 'zinc finger' structure based on protein structure prediction and observed distribution of amino acid residues have been proposed recently [4, 5]. Unfortunately, although several groups have been trying, convincing experimental support is still lacking. Indeed, crystallisation has been so far unsuccessful and aggregation and/or precipitation make the studies in solution difficult.

A low-resolution three-dimensional structure of the 'zinc fingers' from yeast alcohol dehydrogenase regulatory gene *ADR1* as determined by two-dimensional ^{1}H-NMR spectroscopy was published recently [6]. The structure shows as a prominent feature an α helix between residues Leu17 and Lys24, but no evidence for the β-hairpin structure predicted from modeling studies [4, 5] was found.

In this paper, we present the structure of a 'zinc finger' domain from a different source, as determined by two-dimensional NMR, distance geometry and restrained molecular dynamics (RMD). The 30-amino-acid peptide is a single domain from the mouse Kruppel-like gene (*mKr2*) [7] with the sequence EKPYECTECGKAFSQSAYLIEHRRIHTGEK. In this sequence, the conserved hydrophobic residues correspond to Tyr4, Phe13 and Leu19 [2]. The product of *mKr2* is probably a regulatory factor required for differentiation and/or phenotypic maintenance of neurons, since *mKr2* transcripts were detected in all major structures of the nervous system during embryogenesis [7]. We show here that it is possible to overcome the experimental difficulties by determining the structure of the 'zinc finger' without the zinc and showing that the structure found in these conditions could still bind zinc without major structural rearrangements.

MATERIAL AND METHODS

The 30-residue peptide incorporating the seventh 'zinc finger' domain from *mKr2* was synthesised in a continuous flow instrument using 9-fluorenyl-methyl-oxycarbonyl chemistry and *in situ* activation with Castro's reagent (1-benzotriazolyl-*N*-oxy-tris(dimethylamino)phosphonium hexafluorophosphate) as described earlier [8] and then purified by reverse-phase high-performance liquid chromatography.

The NMR experiments were performed on a Bruker AM 500 spectrometer with a proton resonance frequency of 500 MHz. Two-dimensional double quantum filtered correlated spectroscopy (DQF-COSY) [9, 10], nuclear Overhauser enhancement spectroscopy (NOESY) [11, 12] and rotating frame nuclear Overhauser enhancement spectroscopy (ROESY) [13–15] were performed in the phase-sensitive mode. Quadrature detection in the ω_1 dimension was obtained using time-proportional phase incrementation [16]. The relay

Correspondence to P. Roesch, Max-Planck-Institut für Medizinische Forschung, Abteilung Biophysik, Jahnstrasse 29, D-6900 Heidelberg, Federal Republic of Germany

Abbreviations. ADR1, alcohol dehydrogenase regulatory gene; COSY, correlated spectroscopy; DQF, double quantum filtered; *mKr2*, mouse Kruppel-like gene; NOE, nuclear Overhauser effect; NOESY, nuclear Overhauser enhancement spectroscopy; ROESY, rotating frame NOESY; RELAY, relayed coherence transfer spectroscopy.

Note. During the processing procedure for this manuscript, Peter Wright and coworkers published the solution structure of a different synthetic zinc-finger peptide, corresponding to a motif from the *Xenopus* protein Xfin, in the presence of zinc ions [Lee et al. (1989) *Science 245*, 635–637]. Lee et al. obviously did not encounter problems with precipitation of the peptide in the presence of zinc at pH values above 5 as we did. Their structure seems to be better defined from the experimental data and is closer to the theoretical structure predictions for the general zinc-finger motif than the one we present in this paper.

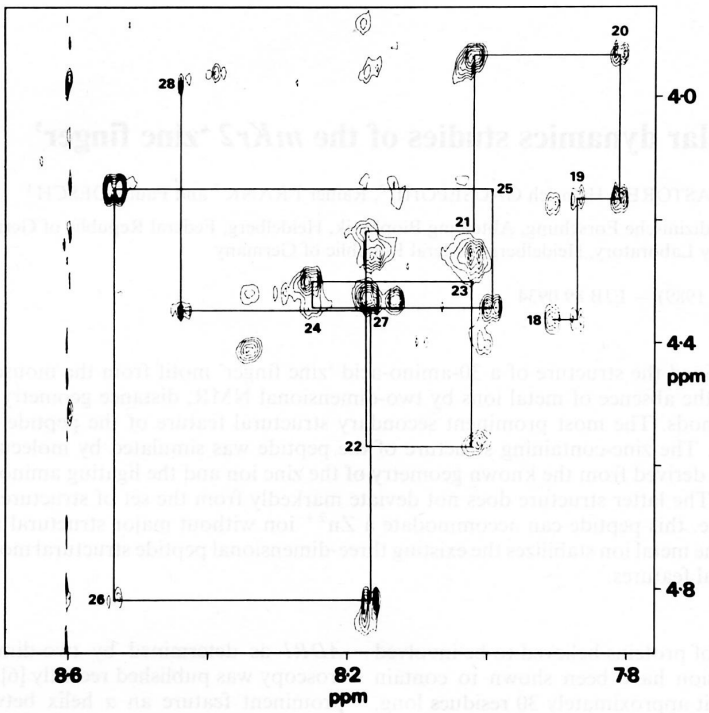

Fig. 1. *Fingerprint region from a phase-sensitive NOESY spectrum of the* mKr2 *'zinc finger'*. The figure shows the sequential assignments, via NH to CαH ($i, i+1$), for a decapeptide segment beginning at Tyr18. Mixing time, $s = 350$ ms

coherence transfer (RELAY) [17, 18] spectra were acquired in magnitude mode. In the majority of measurements the signal from water was suppressed by selective, on resonance, irradiation which was applied at all times except during acquisition. However, in some NOESY experiments water suppression was achieved by placing the carrier on resonance and using a modified NOESY sequence in which the last 90° pulse was replaced by a semi-selective 90°-τ-90° 'jump and return' pulse ($\tau = 125$ μs) [19].

All NMR measurements were carried out at 35°C, with 128 or 176 scans being collected at each of the 512 t_1 increments. A sweep width of either 4166.67 Hz or 4504.50 Hz was used in both dimensions with the carrier positioned in the centre of the spectrum. Prior to Fourier transformation the original data sets of 4 K by 512 W were zero-filled to 4 K by 2 K and then multiplied in both dimensions by a shifted sine-bell function in order to improve resolution in the final spectra.

DQ-COSY, RELAY ($s = 18$ ms) and NOESY experiments ($t_m = 200$ ms and 300 ms) were collected from 5-mM samples of the 'zinc finger' dissolved in both 100% D_2O and 90% H_2O/10% D_2O adjusted to pH 3. In addition, a NOESY spectrum with a longer mixing time of 350 ms was acquired from 90% H_2O/10% D_2O solutions of the 'zinc finger'. The ROESY spectra were obtained using a spin lock field of 2.8 kHz.

Metric matrix distance geometry calculations were carried out with the DISGEO program [20–22]. 20 structures were calculated using 86 NMR restraints, 41 of which were medium and long range, and coupling constant information where possible (e.g. in the helical region). Peak intensities were judged from contour plots of NOESY spectra (mixing time $\tau = 300$ ms), where successive contour levels were spaced by 2^n. The evaluation of cross peaks from spectra with shorter mixing times was not possible because of the low cross-peak intensities. Distances were calibrated into three classes: strong (0.26 nm), medium (0.35 nm) and weak (0.45 nm). The standard corrections were also added to the distances where the use of pseudoatoms [23] was necessary. An additional correction (0.05 nm) was used for the methyl groups, to take into account the spin-system multiplicity. Experiments in D_2O and in H_2O needed independent calibrations.

All the energy minimization and molecular dynamics calculations were carried out by using the GROMOS package [24, 25]. The potential energy function describing the atomic interactions included terms representing covalent-bond stretching, bond-angle bending, harmonic dihedral bending, sinusoidal dihedral torsion, van der Waals and Coulomb interactions.

Bond-length constraints were applied by using the SHAKE algorithm [26, 27]. To reduce the number of van der Waals interaction pairs considered in the restrained molecular dynamics and in the energy minimisation runs, interactions were neglected when the atomic separation became greater than 0.8 nm and the list of interactions considered was updated every 10 steps of 2 fs. In the RMD runs, the system was weakly coupled to a thermal bath of $T = 300$ K with a temperature relaxation time of 0.01 ps during the first 2 ps and 0.8 ps for all the following runs. The initial velocities for the atoms were taken from a random Maxwellian distribution at 300 K. Only the last 10 ps were considered in the calculation of the averaged structures and the average was further minimised with 500 cycles of energy minimisation.

The interproton NMR distance restraints from nuclear Overhauser effect (NOE) data were included as a semi-harmonic potential function with a force constant which increased slowly over the range $500-2000$ kJ · nm^{-2} · mol^{-1}

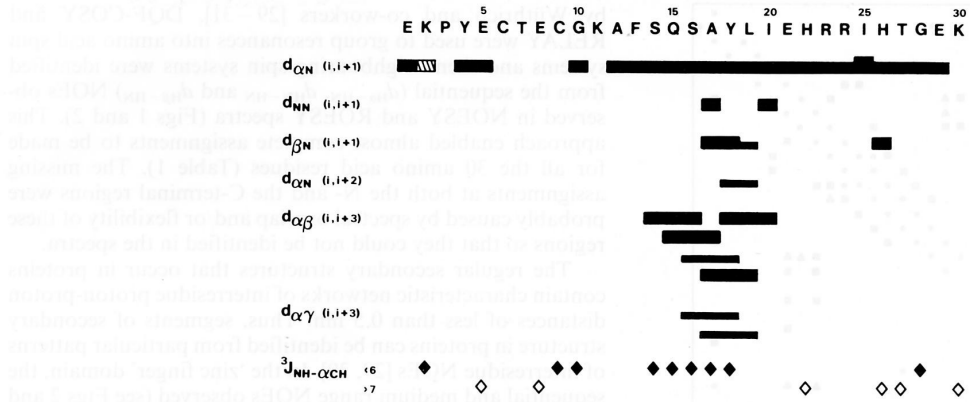

Fig. 2. *Summary of interresidue NOEs and* $^3J_{NH-C\alpha H}$ *coupling constants used to determine the secondary structure of the 'zinc finger' domain.* The bar height is an indication of the NOE intensity. The hatched NOE refers to the δ protons of Pro3 rather than a Cα proton

Table 1. *Chemical shifts of the assigned* ^{1}*H-NMR lines of 'zinc finger' peptide*

Position	Amino acid	Chemical shift of						
		NH	CαH	CβH	CγH	CδH	CεH	CξH
		ppm						
1	Glu		4.08		2.42			
2	Lys	8.63	4.60	1.70, 1.68		1.61	2.96	
3	Pro	–			2.00	3.80, 3.80		
4	Tyr	8.06	4.49	3.02, 2.94		6.82	7.13	
5	Glu	7.94	4.35	3.04	2.39			
6	Cys	8.17	4.49	2.92				
7	Thr	8.54	4.20	4.25	1.19			
8	Glu	8.12	4.29	2.07	2.10			
9	Cys	8.00	4.43	2.86				
10	Gly	8.39	3.95					
11	Lys	8.02	4.42	2.21	1.40	1.65	2.96	
12	Ala	8.16	4.25	1.21				
13	Phe	8.01	4.55	3.08		7.32[a]	7.23[b]	7.42[c]
14	Ser	8.01	4.41	3.88, 3.81				
15	Gln	8.34	4.32	2.05	2.16			
16	Ser	8.15	4.30	3.90, 3.84				
17	Ala	8.13	4.16	1.33				
18	Tyr	7.91	4.35	3.16, 3.05		6.75	7.02	
19	Leu	7.86	4.15	1.69	1.56	1.60	1.01 0.87	
20	Ile	7.80	3.92	1.84	1.54, 1.16	0.82		
					0.84			
21	Glu	8.02	4.19	1.94	2.12			
22	His	8.17	4.57	3.26 2.82				
					8.62[d]	7.21[e]		
23	Arg	8.16	4.29	1.83, 1.63	1.64	3.17, 7.14		
24	Arg	8.23	4.34	1.77, 1.72	1.52	3.19, 8.05		
25	Ile	7.99	4.14	1.79	1.36, 1.32	0.80		
				0.82				
26	His	8.54	4.79	3.21, 3.18				
					8.53[d]	7.02[e]		
27	Thr	8.16	4.34	4.20	1.16			
28	Gly	8.44	3.96					
29	Glu		4.38					
30	Lys							

[a] C2/6H
[b] C3/5H
[c] C6H
[d] C2H
[e] C4H

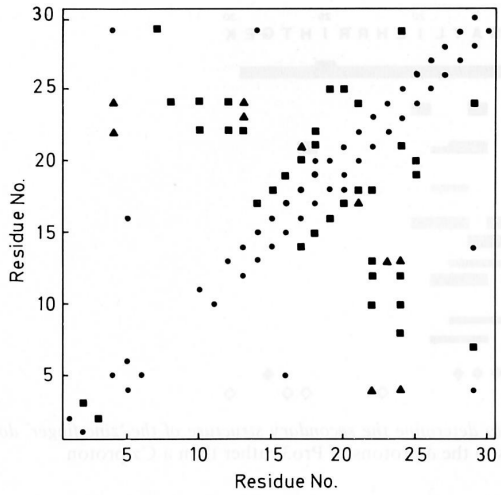

Fig. 3. *A 'diagonal' plot summarising the distribution of the interresidue NOEs observed for the 'zinc finger' domain.* The symbols denote NOEs between backbone protons (●), backbone to sidechains (■) and between sidechains (▲). When several NOEs were observed involving the same residue pair only the one between backbone protons is indicated

Table 2. *Energy contributions during structure refinement*
EM, energy minimisation; MD, molecular dynamics (see text for details); E_{pot}, total potential energy; E_{elec}, electrostatic energy; E_{LJ}, Lennard Jones energy; E_{NOE}, semiharmonic potential with force constant 1000 kJ·mol^{-1}· nm^{-2}

Structure		E_{pot}	E_{elec}	E_{LJ}	E_{NOE}
		kJ/mol			
A1	after DISGEO	10^5	−313	10^5	198
	after EM	−484	−750	−692	328
	after 41 ps MD	−331	−849	−747	191
	after MD + EM	−1348	−963	−944	175
	after MD with Zn	−88	−867	−704	226
B1	after DISGEO	10^5	−303	10^5	187
	after EM	−683	−746	−786	260
	after 41 ps MD	−599	−978	−773	139
	after MD + EM	−1400	−1068	−923	125
	after MD with Zn	−31	−857	−699	240

[28]. This means that an extra potential term appears only if the actual distance between restrained atom pairs exceeds the limit imposed by the NMR data.

In the simulation with the zinc, 12 more restraints were added to reproduce the tetrahedral environment between the zinc and the cysteines and the histidines. In this calculation, the temperature was increased to 500 K for 10 ps in order to provide the system with enough kinetic energy to overcome higher barriers. The system was then slowly cooled down and 10 ps more were calculated. Finally, the structure was again energy-minimised.

All the calculations were carried out on the Vax 8650 of the EMBL in Heidelberg (FRG).

RESULTS AND DISCUSSION

The sequence-specific assignments for the 'zinc finger' domain were carried out using the procedures developed by Wüthrich and co-workers [29–31]. DQF-COSY and RELAY were used to group resonances into amino acid spin systems and then neighbouring spin systems were identified from the sequential ($d_{H\alpha-HN}$, d_{HN-HN} and $d_{H\beta-HN}$) NOEs observed in NOESY and ROESY spectra (Figs 1 and 2). This approach enabled almost complete assignments to be made for all the 30 amino acid residues (Table 1). The missing assignments at both the N- and the C-terminal regions were probably caused by spectral overlap and/or flexibility of these regions so that they could not be identified in the spectra.

The regular secondary structures that occur in proteins contain characteristic networks of interresidue proton-proton distances of less than 0.5 nm. Thus, segments of secondary structure in proteins can be identified from particular patterns of interresidue NOEs [29, 30]. In the 'zinc finger' domain, the sequential and medium range NOEs observed (see Figs 2 and 3) indicate that residues 14–20 or 21 form a short helix. A helical conformation for amino acids 14–18 is also supported by the fact that all these residues have $^3J_{HN-H\alpha}$ coupling constants of less than 6 Hz, which is consistent with the ϕ/ψ backbone angles expected for a helix [32].

In the two predicted 'zinc finger' structures the residues equivalent to 4–13 [4], or 1–14 [5], were proposed to form a β hairpin. We found no NOE or $^3J_{HN-H\alpha}$ coupling constant evidence to suggest such a conformation in the *mKr2* protein finger, in agreement with the study of one of the two 'finger' domains from yeast ADR1 (ADR1a) in solution [6].

Distance restraints and coupling constant information were used as input for distance geometry calculations. 20 runs starting from different choices of the initial distance matrix were performed, of which 13 structures satisfactorily converged. They could be divided into two classes, containing five (class A) and eight (class B) structures, one having the mirror image fold topology of the other. In the two classes, although the helical element was always correctly right-handed, the relative position of the loop and of the helix was inverted. The average root-mean-square deviation within class A was 0.38 nm (all atoms), as compared to 0.31 nm in class B, and 0.25 nm for the backbone atoms only as against 0.20 nm, respectively.

As distance geometry algorithms are purely based on distances and do not take into account energy considerations, the final structures had to be energy-minimised to relieve internal molecular strain and possible bad contacts. The best structure from each class, in terms of both minimal energy and residual violations, was also subjected to further refinement, by calculating 41 ps of restrained molecular dynamics. Table 2 shows the most significant energy terms for the two structures at different stages of the refinement.

Although more experimental data would be necessary to determine the correct topology unambiguously, we suggest class B to have the correct or, at least predominant folding, on the basis of its higher stability, smaller residual violations and better agreement within the class, i.e. lower root-mean-square deviation.

The class B tertiary structure of the *mKr2* protein 'finger' domain obtained as described is shown in Fig. 4 (top). The degree of agreement between the five best converged structures indicates that the NMR data defines a single global fold for the backbone of the 'zinc finger', although some regions are better defined than others (Fig. 4, middle). The helical region is conserved quite well, whilst the conformation of the large loop formed by residues 5–12, which includes the cysteines involved in Zn^{2+} chelation, shows significant variation because of the sparsity of NOEs involving this part of the protein

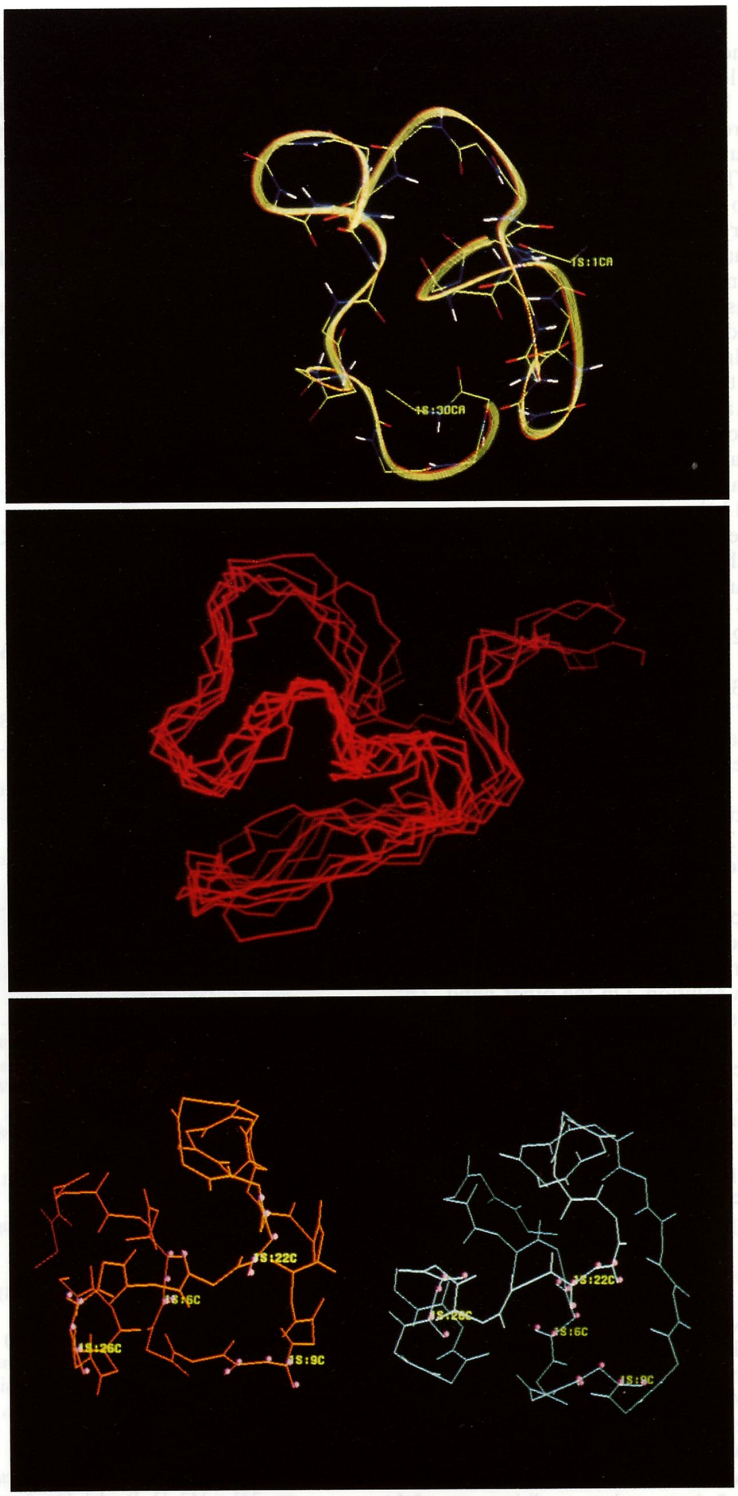

Fig. 4. *Results from DISGEO and molecular dynamics calculations with and without imposing the zinc restraints.* Top: tertiary folding of the 'zinc-finger'-domain peptide backbone with superimposed ribbon based on DISGEO and restrained molecular dynamics calculations. Middle: a family of the 'best' five structures in terms of potential energy and of residual violations on the experimental restraints obtained by DISGEO and energy minimization. They were superimposed minimizing the root-mean-square difference between backbone atoms (averaged root mean square, 0.20 nm). Another family with mirror image topology about the plane formed by the loop involving residues 5—12 was also obtained. It is not possible, at this stage, to decide which of the two classes of structures exists in solution. Bottom: comparison of the zinc-free structure (right) and the structure with additional restraints simulating the zinc coordination (left) as determined by restrained molecular dynamics calculations. The Cys and His residues supposed to be involved in zinc complexation are shown in pink

(see Fig. 3). This is almost certainly a consequence of the relative flexibility of the loop.

The location of the helical region in the *mKr2* protein 'finger domain' differs from the predicted 'zinc finger' structures, where residues equivalent to 18–26 [4], or 15–27 [5], were built as an α helix. The ^{1}H-NMR study of ADR1a also concluded that the amino acids corresponding to 18–25 form an α helix [6]. A secondary structure search on the final *mKr2* protein 'finger' coordinates using the computer program DSSP by Kabsch and Sander [33] suggested that the region of residues 14–20 conforms to the 3_{10} rather than to the α-helix type, although this could not be confirmed by independent experimental evidence. In fact, it is not easy to distinguish experimentally between the two helix types [30]. The NMR measurements on ADR1a were performed with Zn^{2+} bound to the protein, which could account for the differences in structure. However, a change in the secondary structure of the *mKr2* protein 'finger' may not be necessary to accommodate a Zn^{2+} ion, as suggested below.

An interesting feature of this 'zinc finger' structure is that it agrees with many of the known biochemical properties of 'finger' proteins. The structure is fairly compact and globular, which could explain why individual 'zinc fingers' are resistant to proteolytic digestion [2, 34]. The helical region of the 'finger' domain, which is about 0.9 nm in length, could, like other DNA-binding proteins [35] and as proposed for the transcription factor IIIA 'fingers' [1, 36], bind to the major groove of DNA and interact with a group of two or three bases. Also, the hydrophobic residues predicted to form a hydrophobic core of the 'zinc finger' [2] are rather closely spaced in the three-dimensional structure. The distance between the side chain of Tyr4 and Phe13 is approximately 0.4 nm, and the distance between the side chain of Tyr4 and Leu19 approximately 0.6 nm.

On one hand, the experiments reported here demonstrate that the Zn^{2+}-free 'finger' domain clearly possesses a well-defined tertiary structure, although the two mirror image structures may coesist in solution. On the other hand, Zn^{2+} seems to be required for sequence-specific binding of 'fingers' to DNA [2, 34, 37] and to clarify the influence of the Zn^{2+} ion on the peptide structure it is important to consider the structural changes which occur on Zn^{2+} binding. Because the histidines are still protonated, the 'zinc finger' is unable to bind Zn^{2+} at pH 3, as also shown by the identity of one-dimensional ^{1}H-NMR spectra obtained in the presence and absence of $ZnCl_2$. However, experiments at higher pH were not possible since the peptide in the presence of zinc precipitated above pH 5.

To have an indication of the conformational changes needed by our structure to be able to accommodate the zinc ion, we extended the RMD trajectory previously calculated. We simulated the tetrahedral environment of the zinc by adding 12 distances to the experimental restraints and calculating 20 ps of RMD. Although it cannot be considered a description of the solution structure of the fingers with zinc, we wanted to evaluate whether the zinc could be accommodated in our structure without too large rearrangements of the overall folding. Table 2 shows only a small increase of the NOE contribution, supporting our hypothesis. The increase arises from the addition of non-experimental data which could well be not entirely compatible with the NOE distances. As a consequence, distorsions in the geometry lead to an increase of the other energy contributions.

In conclusion, we have shown that a synthetic, Zn^{2+}-free, single 'zinc finger' domain from *mKr2* protein adopts a stable structure in aqueous solution. This supports the view that 'zinc fingers' form independent structural protein domains that could act as nucleic-acid binding sites. The zinc-free structure does not necessarily undergo substantial alterations on Zn^{2+} binding, so that metal-ion complexation is expected to exert only an additional stabilising effect which is nevertheless of crucial importance for sequence-specific DNA binding.

We would like to thank Drs C. Sander and T. Gibson for helpful discussions and Prof. K. C. Holmes for constant encouragement. A. P. would also like to thank Dr M. A. Castiglione Morelli for help and moral support. M. D. Carr was supported by a European Science Exchange Fellowship from the Royal Society of London.

REFERENCES

1. Klug, A. & Rhodes, D. (1987) *Trends Biochem. Sci. 12*, 464–469.
2. Miller, J., McLachlan, A. D. & Klug, A. (1985) *EMBO J. 4*, 1609–1614.
3. Diakun, G. P., Fairall, L. & Klug, A. (1986) *Nature 324*, 698–699.
4. Berg, J. M. (1988) *Proc. Natl Acad. Sci. USA 85*, 99–102.
5. Gibson, T. J., Postma, J. P. M., Brown, R. S. & Argos, P. (1988) *Protein Eng. 2*, 209–218.
6. Parraga, G., Horvarth, S. J., Eisen, A., Taylor, W. E., Hood, L., Young, E. T. & Klevit, R. E. (1988) *Science 241*, 1489–1492.
7. Chowdbury, K., Dressler, G., Breir, G., Deutch, U. & Gruss, P. (1988) *EMBO J. 7*, 1345–1353.
8. Frank, R. & Gausepohl, H. (1988) in *Modern methods in protein chemistry*, vol. III (Tschensche, H., ed.) pp. 41–60, deGruyter, Berlin, New York.
9. Piantini, U., Sorensen, O. W., & Ernst, R. R. (1982) *J. Am. Chem. Soc. 104*, 6800–6801.
10. Shaka, A. J. & Freeman, R. (1983) *J. Magn. Res. 51*, 169–173.
11. Jeener, J., Meier, B. H., Bachman, P. & Ernst, R. R. (1979) *J. Chem. Phys. 71*, 4546–4553.
12. Macura, S., Huang, Y., Suter, D. & Ernst, R. R. (1981) *J. Magn. Res. 43*, 259–281.
13. Bothner-By, A. A., Stephens, R. L., Lee, J., Warren, C. D. & Jeanloz, R. W. (1984) *J. Am. Chem. Soc. 106*, 811–813.
14. Kessler, H., Griesinger, C., Kerssebaum, R., Wagner, K. & Ernst, R. R. (1987) *J. Am. Chem. Soc. 109*, 607–609.
15. Rance, M. (1987) *J. Magn. Res. 74*, 557–564.
16. Marion, D. & Wüthrich, K. (1983) *Biochem. Biophys. Res. Commun. 113*, 967–974.
17. Eich, G., Bodenhausen, G. & Ernst, R. R. (1982) *J. Am. Chem. Soc. 104*, 3731–3732.
18. Bax, A. & Drobny, G. (1985) *J. Magn. Res. 61*, 306–320.
19. Plateau, P. & Gueron, M. (1982) *J. Am. Chem. Soc. 104*, 7310–7311.
20. Havel, T. F. & Wüthrich, K. (1984) *Bull. Math. Biol. 46*, 673–698.
21. Havel, T. F. & Wüthrich, K. (1985) *J. Mol. Biol. 182*, 281–294.
22. Havel, T. F. (1986) DISGEO, Quantum Chemistry Program Exchange No. 507, Indiana University, Bloomington, IN.
23. Wüthrich, K., Billeter, M. & Braun, W. (1983) *J. Mol. Biol. 169*, 949–961.
24. Berendsen, H. J. C., Postma, J. P. M., van Gusteren, W. F. & Hermans, J. (1981) in *Intermolecular forces* (Pullman, B., ed.) pp. 331–342, D. Reidel, Dordrecht, The Netherlands.
25. Van Gunsteren, W. F., Kaptein, R. & Zuiderwerg, E. R. P. (1983) in *Nucleic acid conformation and dynamics* (Olson, W. K., ed.) pp. 79–92, Report of NATO/CECAM Workshop, Orsay, France.
26. Ryckaert, J. P., Ciccotti, G. & Berendsen, H. J. C. (1977) *J. Comp. Phys. 23*, 327–341.
27. Van Gunsteren, W. F. & Berendsen, H. J. C., (1977) *Mol. Phys. 34*, 1311–1327.

28. Van Gunsteren, W. F., Boelens, R., Kaptein, R., Scheek, R. M. & Zuiderwerg, E. R. P. (1985) in *Molecular dynamics and protein structure*, pp. 92–99, Polycrystal Book Service, P.O. Box 27, Western Springs, I-60558, USA.
29. Wagner, G., Braun, W., Havel, T. F., Schaumann, T., Go, N. & Wüthrich, K. (1987) *J. Mol. Biol. 196*, 611–639.
30. Wüthrich, K. (1986) *NMR of proteins and nucleic acids*, John Wiley & Sons, New York.
31. Wüthrich, K., Billeter, M. & Braun, W. (1984) *J. Mol. Biol. 180*, 715–740.
32. Pardi, A., Billeter, M. & Wüthrich, K. (1984) *J. Mol. Biol. 180*, 741–751.
33. Kabsch, W. & Sander, C. (1983) *Biopolymers 22*, 2577–2637.
34. Frankel, A. D., Berg, J. M. & Pabo, C. O. (1987) *Proc. Natl Acad. Sci. USA 84*, 4841–4845.
35. Anderson, J. E., Ptashne, M. & Harrison, S. C. (1987) *Nature 326*, 846–852.
36. Fairfall, L., Rhosdes, D. & Klug, A. (1986) *J. Mol. Biol. 192*, 577–591.
37. Nagai, K., Nakaseko, Y., Nasmyth, K. & Rhodes, D. (1988) *Nature 332*, 284–286.